Contents lists available at ScienceDirect

Journal of Controlled Release

Visualizing disintegration of 3D printed tablets in humans using MRI and comparison with in vitro data

Iria Seoane-Viaño [a,b,1], Tania Pérez-Ramos [c,1], Jiaqi Liu [a], Patricija Januskaite [a], Elena Guerra-Baamonde [c], Jorge González-Ramírez [c], Manuel Vázquez-Caruncho [c,**], Abdul W. Basit [a,d,*], Alvaro Goyanes [a,d,e,*]

[a] Department of Pharmaceutics, UCL School of Pharmacy, University College London, 29-39 Brunswick Square, London WC1N 1AX, UK
[b] Department of Pharmacology, Pharmacy and Pharmaceutical Technology, Paraquasil Group (GI-2109), Faculty of Pharmacy, iMATUS and Health Research Institute of Santiago de Compostela (IDIS), University of Santiago de Compostela (USC), Santiago de Compostela 15782, Spain
[c] Radiology Department, University Hospital Lucus Augusti (HULA), Rúa Dr. Ulises Romero, 1, Lugo 27003, Spain
[d] FabRx Ltd., Henwood House, Henwood, Ashford TN24 8DH, UK
[e] Departamento de Farmacología, Farmacia y Tecnología Farmacéutica, I+D Farma Group (GI-1645), Facultad de Farmacia, iMATUS and Health Research Institute of Santiago de Compostela (IDIS), Universidade de Santiago de Compostela (USC), Santiago de Compostela 15782, Spain

ARTICLE INFO

ABSTRACT

Three-dimensional (3D) printing is revolutionising the way that medicines are manufactured today, paving the way towards more personalised medicine. However, there is limited in vivo data on 3D printed dosage forms, and no studies to date have been performed investigating the intestinal behaviour of these drug products in humans, hindering the complete translation of 3D printed medications into clinical practice. Furthermore, it is unknown whether conventional in vitro release tests can accurately predict the in vivo performance of 3D printed formulations in humans. In this study, selective laser sintering (SLS) 3D printing technology has been used to produce two placebo torus-shaped tablets (printlets) using different laser scanning speeds. The printlets were administered to 6 human volunteers, and in vivo disintegration times were assessed using magnetic resonance imaging (MRI). In vitro disintegration tests were performed using a standard USP disintegration apparatus, as well as an alternative method based on the use of reduced media volume and minimal agitation. Printlets fabricated at a laser scanning speed of 90 mm/s exhibited an average in vitro disintegration time of 7.2 ± 1 min (measured using the USP apparatus) and 25.5 ± 4.1 min (measured using the alternative method). In contrast, printlets manufactured at a higher laser scanning speed of 130 mm/s had an in vitro disintegration time of 2.8 ± 0.8 min (USP apparatus) and 18.8 ± 1.9 min (alternative method). When tested in humans, printlets fabricated at a laser scanning speed of 90 mm/s showed an average disintegration time of 17.3 ± 7.2 min, while those manufactured at a laser scanning speed of 130 mm/s exhibited a shorter disintegration time of 12.7 ± 6.8 min. Although the disintegration times obtained using the alternative method more closely resembled those obtained in vivo, no clear correlation was observed between the in vitro and in vivo disintegration times, highlighting the need to develop better in vitro methodology for 3D printed drug products.

1. Introduction

The manufacturing of solid oral medicines, primarily through tableting and capsule filling, has remained largely unchanged for decades. However, in recent years, innovative technologies such as three-dimensional (3D) printing have landed in the pharmaceutical arena to disrupt the way medicines are manufactured today [1–4]. Among the different 3D printing technologies, selective laser sintering (SLS) stands out as a promising option for implementation in a clinical setting. SLS offers several benefits, including its user-friendly nature and rapid manufacture of Printlets™ (3D printed tablets). One notable advantage is its ability to use commonly employed excipients in conventional tablet

---

manufacturing [5,6]. This compatibility with materials that are well-established in the field of pharmaceuticals greatly streamlines the manufacturing process, encouraging the widespread adoption of SLS in pharmaceutical production [7].

The working principle of SLS 3D printing involves the use of a laser to selectively sinter powdered particles, creating a three-dimensional object layer-by-layer. After the first layer is complete, a blade or roller deposits additional powder on top of the previous layer, and the process is repeated until the desired structure is formed [8,9]. This layer-by-layer approach allows for precise control over the final product's shape and geometry. A unique aspect of SLS is the possibility to change the laser scanning speed to achieve different properties in the printed objects [10,11]. By increasing the laser scanning speed, for example, more porous structures can be obtained, leading to faster disintegration times. Conversely, reducing the scanning speed prolongs the laser's exposure to the powder bed, resulting in denser objects with longer disintegration times [12–14].

The disintegration of oral dosage forms is widely recognised as a crucial stage in facilitating drug release and subsequent absorption. Disintegration testing has gained paramount importance as a quality control measure in the field of pharmaceutical development, particularly for immediate release dosage forms [10,15]. Although complete disintegration does not imply complete dissolution, the simplicity and practicality of disintegration testing make it an appealing technique for assessing dosage form performance. However, there remains a lack of comprehensive harmonization among different pharmacopoeias regarding in vitro disintegration test procedures. This discrepancy can be attributed, at least in part, to the historical emphasis and allocation of resources towards dissolution testing [16,17].

Moreover, while extensive research has been conducted to investigate the in vivo disintegration times and gastric transits of conventional oral formulations using imaging techniques, studies focusing on the behaviour of printlets in vivo have not yet been performed [18–23]. The unique characteristics and complex structures of printlets necessitate a deeper understanding of their disintegration profiles to ensure optimal drug release and absorption. It is crucial to conduct studies that enhance our understanding of the behaviour of the printlets in vivo, enabling informed decisions during drug development and ensuring optimal therapeutic outcomes for patients.

Magnetic resonance imaging (MRI) stands as one of the most frequently utilised imaging techniques to evaluate the gastric transit and intestinal behaviour of dosage forms [24]. MRI offers real-time visualization of the environment surrounding the dosage form, such as stomach water content and intestinal wall contractions [25]. This unique capability makes MRI highly suitable for assessing the in vivo disintegration of oral dosage forms, providing a comprehensive understanding of their behaviour within the gastrointestinal tract [26,27]. By continuously capturing images at various time intervals, clinicians and researchers can observe and analyse the sequential changes in the dosage form's structure and integrity. This dynamic evaluation allows for a more precise assessment of the disintegration kinetics, providing valuable information about the timing and extent of disintegration.

In this study, torus placebo printlets were prepared using SLS 3D printing, followed by an evaluation of their in vivo disintegration time in 6 human volunteers. The selection of the torus shape was based on a previous study that assessed patient acceptability of various 3D-printed oral dosage forms with different shapes, showing that the torus shape was one of the most accepted in terms of swallowability [28]. To accomplish this, two different formulations were printed by employing different laser scanning speeds and incorporating an MRI contrast agent, manganese (II) chloride tetrahydrate, into their composition. In addition to the in vivo studies, in vitro disintegration tests were also conducted using two different setups. The conventional approach involved the utilisation of the United States Pharmacopoeia (USP) disintegration apparatus, a widely employed tool in pharmaceutical testing. The results obtained from this method were then compared with those obtained

when the disintegration test was performed in petri dishes. By combining both in vivo and in vitro studies, a comprehensive understanding of the printlets disintegration behaviour was achieved, providing valuable insights into their disintegration process in real-time. The comparison between the conventional disintegration apparatus and the petri dish method allowed for an assessment of the reliability and consistency of the different testing approaches.

2. Materials & methods

2.1. Materials

Hydroxypropyl cellulose (HPC) grades -L (140,000 g/mol), -SL (100,000 g/mol), -SSL (40,000 g/mol), and -UL (20,000 g/mol) were obtained from NISSO (Tokyo, Japan). Candurin® Gold Sheen was purchased from Merck KGaA (Darmstadt, Germany). Manganese (II) chloride tetrahydrate ($MnCl_2$) FCC grade was obtained from Cenic Chemicals Ltd. (Vale of Glamorgan, UK). Iron (III) oxide was obtained from Fisher Scientific (Leicestershire, UK). Iron (II) sulfate heptahydrate and ammonium iron (III) citrate were obtained from Sigma-Aldrich (Dorset, UK). Fumed Silica was purchased from Evonik Industries AG (Essen, Germany).

2.2. SLS 3D printing for preliminary studies

Preliminary studies were conducted to choose the most adequate HPC polymer grade and MRI contrast agent. Firstly, the best contrast agent was evaluated. A total amount of 30 g of HPC-UL, Candurin® Gold Sheen and the MRI contrast agent were mixed using a mortar and pestle for each formulation (Table 1). The MRI contrast agents and HPC powder were sieved through a 180 μm sieve prior to mixing, except for the $MnCl_2$ and fumed silica. $MnCl_2$ was ground into a fine powder before blending while fumed silica was added directly into the formulation. HPC was chosen as the main excipient due to its swelling capacity, acting as a disintegrant [29]. To increase energy absorption from the laser and aid printability, 3% of Candurin® was added to the formulations [30,31]. After blending, the placebo pharma-inks were transferred to the SLS printer (Sintratec Kit, AG, Brugg, Switzerland). A cylindrical printlet template (12.76 mm width x 3.9 mm height) was designed using 123D Design (Version 14.2.2, Autodesk Inc., San Rafael, CA, USA). The 3D model was exported as a stereolithography (.stl) file into the 3D printer Sintratec central software (Version 1.1.13, Sintratec, AG, Brugg,

Table 1
Printlets with variousMRI contrast agents and printing parameters. All formulations contained 3% w/w Candurin® Gold Sheen.

Formulation	HPC-UL (% w/w)	MRI contrast agent	Chamber Temperature (°C)	Surface Temperature (°C)	Laser Speed (mm/s)
HPC-blank	97	–	80	100	100
HPC-FeO	92	5% Iron (II) Oxide	80	100	100
HPC-Fe$_2$O$_3$	92	5% Iron (III) Oxide	80	100	100
HPC-FeSO$_4$	92	5% Iron (II) Sulfate	80	100	100
HPC-SiO$_2$	92	5% Fumed Silica	90	110	50
HPC-NH$_4$Fe(SO$_4$)$_2$	92	5% Ammonium Iron (III) Citrate	80	100	100
HPC-MnCl$_2$	92	5% Manganese (II) Chloride	80	100	100

Switzerland). The cylindrical printlet shape was chosen for the preliminary studies due to its simplicity.

The powdered pharma-ink in the platform reservoir (150 × 150 × 150 mm) of the printer was moved by a sled to a building platform (150 × 150 × 150 mm) creating a flat and homogeneously distributed layer of powder. For most of the formulations in Table 1, a surface temperature of 100 °C and a chamber temperature of 80 °C were chosen, whereas for the fumed silica group a surface temperature of 110 °C and a chamber temperature of 90 °C were selected. The 2.3 W blue diode laser (445 nm) sintered the pharma-ink on the building platform in a pre-defined pattern based on the .stl file. Then, the reservoir platform moved up, the building platform moved down, and the sled distributed a thin layer of pharma-ink powder on top of the previous layer. This process was repeated layer-by-layer until completion. Printlets were then removed from the powder bed and any excess powder was brushed off.

At this point, the use of HPC-UL was discontinued due to its tendency to cause the powder distribution roller to get stuck when using HPC-UL mixed with the contrast agents, something that did not happen with the other HPC grades. As a result, the three remaining HPC grades were tested at varying laser scanning speeds (50, 75, 100 and 125 mm/s) (Table 2). These powder blends did not contain any MRI contrast agent. During each print, four printlets were simultaneously created.

The optimum HPC grade and the best MRI contrast agent and were identified from previous steps. Next steps included the formulation of printlets with the optimal combination of excipients using various laser scanning speeds, as shown in Table 3.

2.3. Scanning electron microscopy (SEM)

Scanning electron microscopy (SEM) images were obtained using a JSM-840 A scanning electron microscope (JEOL GmbH, Germany). Images of the surface and the cross-section of printlets in Tables 2 and 3 were taken after coating with carbon (~30–40 nm).

2.4. In vitro MRI scan

The seven formulations listed in Table 1 were introduced into a multi-well plate. Water was then added to the wells containing the formulations, and subsequent T1 and T2-weighted FIESTA sequences were conducted using a SIGNA™ Explorer MR system (GE Healthcare, Madrid, Spain). Prior to the MRI scan, photographs were taken to capture the initial state of the samples, and after the scan, additional photographs were taken to document any changes observed.

Table 2
Printlets prepared with different HPC grades and varying laser scanning speeds. All formulations contained 97% w/w HPC polymer and 3% w/w Candurin® Gold Sheen.

Formulation	HPC grade	Chamber Temperature (°C)	Surface Temperature (°C)	Laser Speed (mm/s)
HPC-SSL 50	SSL	80	100	50
HPC-SSL 75	SSL	80	100	75
HPC-SSL 100	SSL	80	100	100
HPC-SSL 125	SSL	80	100	125
HPC-SL 50	SL	80	100	50
HPC-SL 75	SL	80	100	75
HPC-SL 100	SL	80	100	100
HPC-SL 125	SL	80	100	125
HPC-L 50	L	80	100	50
HPC-L 75	L	80	100	75
HPC-L 100	L	80	100	100
HPC-L 125	L	80	100	125

Table 3
Printlets prepared using the optimal combination of excipients at different laser scanning speeds.

HPC-SSL (% w/w)	$MnCl_2$ (% w/w)	Candurin® Gold Sheen (% w/w)	Chamber Temperature (°C)	Surface Temperature (°C)	Laser Speed (mm/s)
92	5	3	80	100	50
92	5	3	80	100	75
92	5	3	80	100	100
92	5	3	80	100	125

2.5. In vitro preliminary disintegration study

The in vitro disintegration behaviour of the 3D printed cylindrical tablets was tested in 900 mL of 0.1 M hydrochloric acid at 37 ± 0.5 °C using the USP disintegration apparatus (ZT43, Copley, UK). Each printlet was placed on the basket rack assembly and a perforated disc was placed on top of it. Disintegration was regarded as completed when the printlets lost their original form and the components separated. To obtain an average value, three printlets were disintegrated for each group listed in Table 2 and Table 3.

2.6. SLS 3D printing for in vivo and in vitro disintegration studies

Once the most suitable HPC polymer grade and contrast agent were chosen, the final printlets were prepared. To prepare the pharma-inks (Table 4), a total amount of 100 g of HPC-SSL, $MnCl_2$, and Candurin® Gold Sheen was mixed using a mortar and pestle. The HPC powder was sieved through a 180 μm sieve prior to mixing, whilst the $MnCl_2$ was ground into a fine powder before blending.

Placebo pharma-ink powders were again transferred to a desktop SLS printer to fabricate the placebo oral dosage forms. 123D Design was used to design the templates of the torus printlets (11.5 mm diameter × 5.5 mm height) (Fig. 1). Subsequently, 3D models were exported as an .stl file into the 3D printer Sintratec central software. Torus printlets were fabricated using the same method as the preliminary study cylindrical printlets mentioned previously (section 2.2.) with the printing parameters in Table 4. A total of 6 printlets were made after each print.

2.7. Determination of printlet morphology

The dimensions (diameter and thickness) of the torus printlets were measured using a digital Vernier calliper (GNW Instrumentation, Southport, UK). A Sartorius Entris 124-1S analytical balance (Sartorius AG, Gottingen, Germany) was used to determine the mass of each printlet.

2.8. In vitro disintegration study of SLS torus printlets

The in vitro disintegration behaviour of the torus printlets was tested in the same way as previously stated (section 2.5.). An additional disintegration test was carried out in petri dishes containing 50 mL of 0.1 M hydrochloric acid at 37 ± 0.5 °C without agitation. Each torus (n = 3) was placed in the centre of the petri dish and disintegration was regarded as achieved when the printlets lost their form and the

Table 4
Torus printlet printing parameters for disintegration studies. Both formulations contained 92% w/w HPC-SSL, 5% w/w $MnCl_2$, and 3% w/w Candurin® Gold sheen.

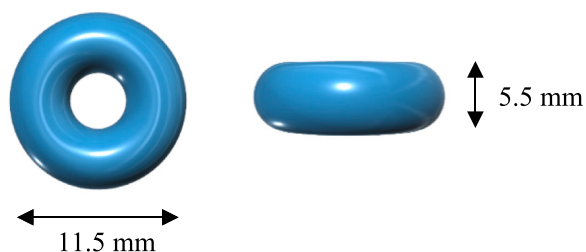| Formulation	Chamber Temperature (°C)	Surface Temperature (°C)	Laser Speed (mm/s)
SLS90	85	105	90
SLS130	85	105	130

Fig. 1. 3D design of the torus printlets.

components separated.

2.9. In vivo study design

The study was conducted as an observational, crossover, prospective, single-center study at the Radiology Department of the University Hospital Lucus Augusti (HULA), Lugo, Spain. The study protocol was checked and approved by the Autonomous Ethical Committee for Clinical Research (CEIC) of Galicia (Spain); registered with code 2021/136.

The 6 participants were healthy adult volunteers of both sexes, with no pathologies or known hypersensitivity to any of the excipients used in this study. All volunteers gave written informed consent and presented no contraindications to MRI. Each volunteer took each placebo formulation on a different day, both at least 7 days apart. Participants were asked to fast for 6 h prior to the MRI acquisitions. The study comprised of the following steps. Firstly, the participants were asked to drink 250 mL of still water (pH = 7.53, hardness = 100 mg/L CaCO$_3$) with the printlets just before entering the MRI machine, to enhance MRI visualization and aid the tracking of the disintegration behaviour. Volunteers underwent an initial sequence of axial, coronal, and sagittal location scanning, and each acquisition was repeated every 90 s until the formulation was no longer seen.

2.10. MRI acquisition and image analysis

Participants were scanned in a supine position (subject lying on their back, head forward) in a SIGNA™ Explorer MR system (GE Healthcare, Spain) or in a SIGNA™ HDxt MR system (GE Healthcare, Madrid, Spain), both with a field strength of 1.5 Tesla in the Radiology Department of the University Hospital Lucus Augusti (HULA), Spain. An 8-channel receiver was placed around the abdomen of the participants and a T2-weighted FIESTA sequence was used since with this sequence the susceptibility artifact generated by the printlets can be detected. Axial, coronal, and sagittal image slices were obtained, and the subjects were allowed to breathe freely during the acquisition. Images were obtained prior to the ingestion of the printlet and after the ingestion with 250 mL of water. The overall duration of image acquisition was ~30 min. Image analysis was performed using Sectra Workstation IDS7 (Sectra AB, Linköping, Sweden). All recordings were evaluated by two independent observers.

Printlet disintegration was observed as loss of torus shape of the characteristically shaped susceptibility artifact in the stomach. Spreading of the artifact was also rated as disintegration of the torus printlet, since for this to happen the printlet needed to disintegrate to such an extent that MnCl$_2$ could disperse into the surrounding medium.

3. Results & discussion

3.1. Preliminary studies

Preliminary studies were conducted to select the most suitable contrast agent to visualise the printlets during in vitro and in vivo MRI. Seven different formulations incorporating different contrast agents (Table 1) were successfully prepared using SLS 3D printing. The diverse colours of the printlets are the result of incorporating MRI contrast agents or by adding the colorant Candurin® Gold sheen. Since the USP apparatus cannot be placed inside the conventional MRI equipment, the traditional disintegration tester was incompatible with the MRI scanner. Therefore, the disintegration test was conducted in water using a multi-well plate. This approach allowed for visualization of the disintegration performance during the MRI scan.

Furthermore, HPC-SiO$_2$, which included 5% fumed silica, was produced at a lower laser speed and higher temperature compared to other formulations (Table 1). This was necessary due to the high viscosity and extremely low bulk density of the fumed silica powder, which adversely affected the quality of the printed object [32]. To create a dense tablet that was not too fragile, the fumed silica powder required more laser energy and higher temperatures for effective sintering. This is because fumed silica has a high melting point and is a poor conductor of heat. It should be noted that in all tablets containing MRI contrast agents, the content ratio of each contrast agent was maintained at 5% *w/w*. Attempts were made with a higher content ratio of 10% w/w, but they were unsuccessful.

MRI scans were conducted during the disintegration process for all formulations (Fig. S1). Notably, formulation HPC-FeO generated a printlet that hindered the visualization of the in vitro disintegration process. Consequently, it was excluded from further research. This was expected since iron (II) oxide is a ferromagnetic compound known to cause significant signal interference in MRI scans [33].

Formulations HPC-Fe$_2$O$_3$, HPC-SiO$_2$ and HPC-NH$_4$Fe(SO$_4$)$_2$ exhibited well-defined shadows in the MRI images, whilst the MRI image of formulation HPC-MnCl$_2$ was completely obscured by a shadow (Fig. S1 B). However, formulations HPC-Fe$_2$O$_3$, HPC-SiO$_2$ and HPC-NH$_4$Fe(SO$_4$)$_2$ remained undissolved throughout the disintegration study, whereas the printlet from formulation HPC-MnCl$_2$ had already completely disintegrated before the MRI scan. Consequently, the shaded region in the MRI image of formulation HPC-MnCl$_2$ was precisely delineated and verified, indicating the presence of the printlet. In line with the research objective of creating disintegrating tablets, formulation HPC-MnCl$_2$ emerged as the preferred choice, with MnCl$_2$ identified as the optimal contrast agent for this study.

The next step involved the selection of the most adequate HPC polymer grade. SLS 3D printing successfully produced cylindrical tablets using three different HPC grades: HPC -SSL, -SL, and -L. The printing process involved four different laser speeds: 50, 75, 100, and 125 mm/s. By incorporating Candurin® Gold sheen, a safe and commonly used colorant, the resulting printlets exhibited a yellow colour. The amount of colorant used was set at 3% *w/w* based on a previous study [34], and was chosen to aid laser absorption.

Printlets prepared at a lower scanning speed (50 mm/s) resulted in a smaller thickness due to excessive energy absorption from the laser, caused by the extended interaction time of the laser with the particles. This prolonged interaction led to complete melting of the materials and subsequent infiltration of molten polymer into the gaps between powder particles. As a result, material delamination was reduced, and printlet density increased. As the laser speed was increased (to 75 mm/s), energy transmission decreased, resulting in a higher porosity and thickness. However, at even higher laser speeds (100 and 125 mm/s), the reduced energy input from the laser led to less formation of necks between particles. This, in turn, resulted in a lower number of layers and a reduction in the final printlet thickness.

HPC grades possess varying viscosities and molecular weights [35]. HPC-SSL has the smallest molecular weight and lowest viscosity, whilst HPC-L has the largest molecular weight and highest viscosity, with HPC-SL falling in between. The molecular weight of HPC determines its viscosity. A polymer with a higher molecular weight has greater molecular chain entanglement, resulting in increased flow resistance and viscosity. Hence, HPC-SSL has the lowest viscosity. Its lower viscosity enhances powder flowability, leading to homogeneous powder distribution and better powder utilisation during the SLS printing process.

Fig. 2 shows that the surface of the HPC-SSL tablet exhibited a uniform and smooth appearance after the addition of $MnCl_2$. This effect can be attributed to the small particle size of the ground $MnCl_2$ powder and its blending with the relatively larger HPC particles, which enhanced printability and resulted in a flatter surface. Specifically, larger particles required higher laser power for melting, which hindered sintering, whilst smaller particles tended to adhere and agglomerate, compromising powder flowability and printability [36]. Therefore, a mixture of small and large particles is preferred to facilitate sintering and improve powder flow.

The printlet colour intensity at different laser speeds provided evidence of the energy transfer variation. As shown in Fig. 2, all printlets had a yellow colour, but the printlet produced at a higher laser speed exhibited a lighter yellow sheen, whilst the printlet at a lower laser speed displayed a darker yellow lustre. This distinction was particularly evident in the HPC-SSL printlets at 50 and 75 mm/s. The darker yellow lustre indicated a greater degree of powder particle sintering, as the laser was in contact with the powder particles for longer.

The comparison of SEM images of cross sections of HPC-SSL printlets without $MnCl_2$ at four different laser speeds, as shown in Fig. 3, reveals a noticeable trend. With increasing laser speed, an increase in voids between powder particles can be observed, resulting in more porous printlets. Moreover, at higher laser speeds, individual particles are more easily identifiable within the printlet. This can be attributed to the reduced sintering of powder particles caused by higher laser speeds, which creates additional spaces within the printlet and consequently decreases its density. Ultimately, this may lead to a shorter disintegration time for the printlet [10]. Similarly, the same trend can be observed in the SEM images of HPC-SSL tablets containing $MnCl_2$. The comparison between printlets with and without $MnCl_2$ reveals minimal differences, suggesting that the addition of $MnCl_2$ may have little to no effect on the properties of HPC printlets.

3.2. USP preliminary disintegration testing

Preliminary in vitro disintegration testing shows that increasing the laser speed resulted in a reduction in disintegration time for each HPC grade (Fig. 4). This can be attributed to less sintering occurring within the shortened sintering time, leading to a more porous structure as confirmed by the SEM images [10].The greater porosity facilitated contact between the printlet and the disintegration media, thereby
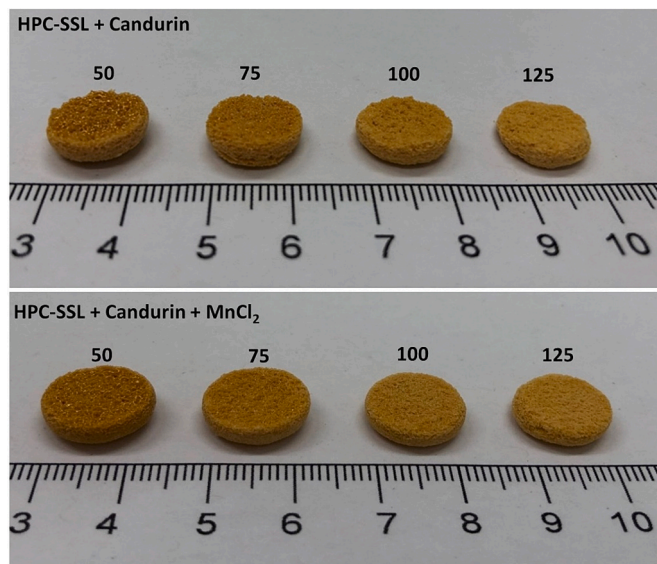

Fig. 2. Comparison of HPC-SSL printlets with and without $MnCl_2$ (numbers above each printlet represent the laser speed in mm/s). Scale is in cm.

accelerating the disintegration time.

A comparison of the disintegration data for printlets prepared using different HPC grades indicate that both HPC -SL and -L printlets exhibited longer disintegration times compared to HPC-SSL printlets at each laser speed. This can be attributed to the lower viscosity of HPC-SSL compared to the other two grades, indicating a faster disintegration rate. As the objective of this research was to manufacture rapidly disintegrating tablets, HPC-SSL was chosen as the most suitable grade of HPC for the in vivo study.

Powder with low viscosity exhibited improved flowability, contributing to the stability of powder delivery and uniform powder distribution at each layer [36]. Consequently, the deposition of powder was homogeneous, allowing for effective sintering of powder particles. On the other hand, powder with high viscosity had poor flowability, leading to uneven powder layer thickness and uneven sintering within the scanning area. This resulted in an inconsistent internal structure of the printlet, where certain parts were excessively sintered while others remained unsintered. Such inhomogeneity within the printlet increased the difficulty of disintegration, thereby prolonging the disintegration time for tablets formulated with a high viscosity HPC grade.

Having determined $MnCl_2$ as the optimal MRI contrast agent and HPC-SSL as the ideal HPC grade, the subsequent phase of this research involved examining the impact of $MnCl_2$ addition on the disintegration behaviour of the printlets. A minimal disparity was observed between the HPC-SSL printlets with and without $MnCl_2$ (Fig. S2). As a result, the incorporation of $MnCl_2$ had no influence on the disintegration performance of HPC-SSL printlets. This finding aligned with the analysis of SEM images, as the porosity of HPC-SSL tablets appeared to be unaltered before and after the addition of $MnCl_2$.

3.3. SLS 3D printing for in vivo MRI and in vitro studies

Based on the findings of the preliminary studies, HPC-SSL was determined to be the optimal choice for HPC grade, whilst $MnCl_2$ was selected as the contrast agent. Torus placebo printlets were successfully produced using SLS 3D printing, employing two different laser speeds: 90 mm/s and 130 mm/s (Fig. 5). The decision to use the torus shape was influenced by a previous study in which the acceptability of 3D printed medicines was evaluated with human volunteers, and the torus shape received the highest acceptance rate in terms of swallowability [28]. The laser scanning speeds, chamber temperature, and surface temperature were determined based on preliminary investigations with the torus shape, although specific data is not presented. The printlets exhibited a consistent shape and size, as shown in Table 5. The SLS90 formulation displayed a greater average weight (167.4 ± 0.013 mg) in comparison to the SLS130 formulation (115.7 ± 0.009 mg), possibly due to its lower porosity structure, as discussed in earlier sections.

To evaluate the in vitro disintegration of the torus printlets, two different disintegration set-ups were employed. Firstly, the conventional in vitro disintegration method described in the USP [37] was followed. The mean disintegration times for the SLS90 and SLS130 formulations were determined to be 7.2 ± 1.0 and 2.8 ± 0.8 min, respectively. Additionally, an alternative in vitro disintegration study was proposed to better simulate conditions found in vivo, by reducing the volume of media (the estimated liquid volume of an empty human stomach is typically around 50 mL to 100 mL) and eliminating intense gastric agitation [25]. For this purpose, the torus printlets were placed in the centre of petri dishes containing 50 mL of HCl 0.1 M at 37 °C. The modified disintegration tests using petri dishes yielded disintegration times of 25.5 ± 4.1 and 18.8 ± 1.9 min for the SLS90 and SLS130 formulations, respectively (Fig. 6). SLS90 printlets exhibited a longer disintegration time compared to SLS130, in line with expectations. Additionally, both SLS90 and SLS130 showed significantly longer disintegration times when using the petri dish setup compared to the USP apparatus.

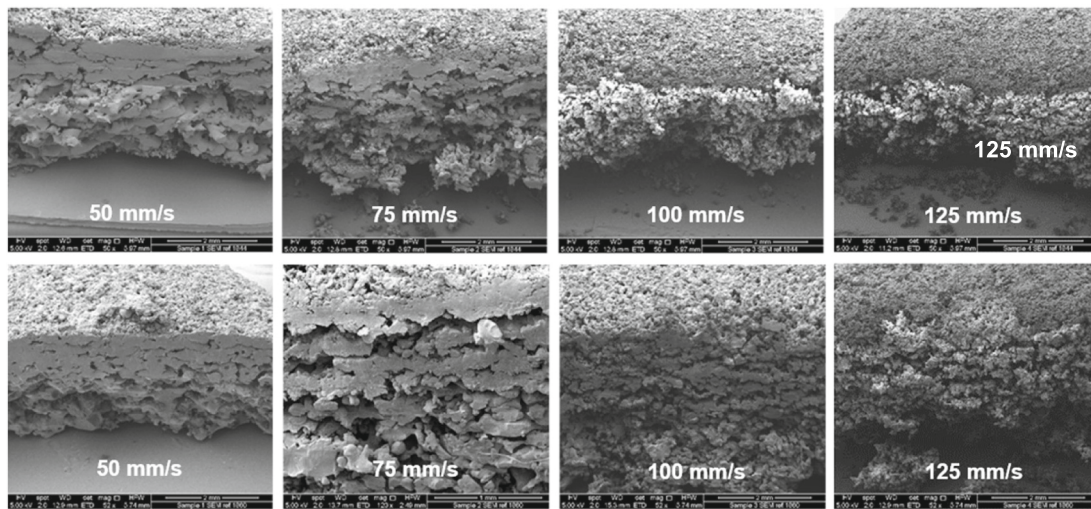MRI was employed to conduct in vivo disintegration studies, as it

Fig. 3. SEM images of cross sections of HPC-SSL printlets, with the top row representing printlets without MnCl$_2$ and the bottom row representing printlets with MnCl$_2$. Different laser speeds are indicated in each image. Scale bar 2 mm.
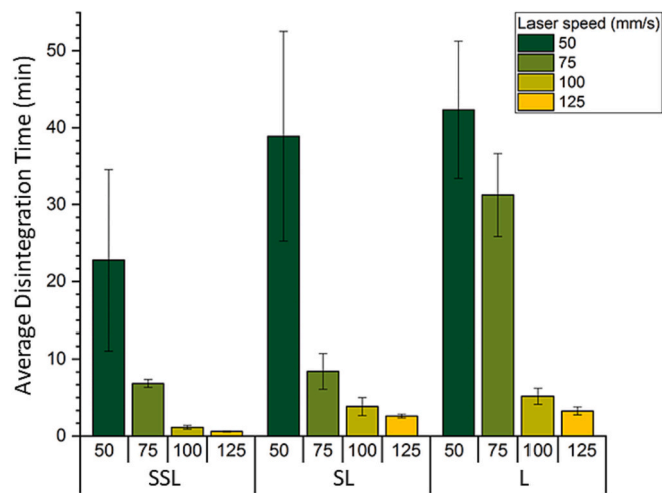

Fig. 4. In vitro disintegration times of printlets prepared using different HPC grades at different laser speeds ($n = 3$). Error bars represent standard deviation.
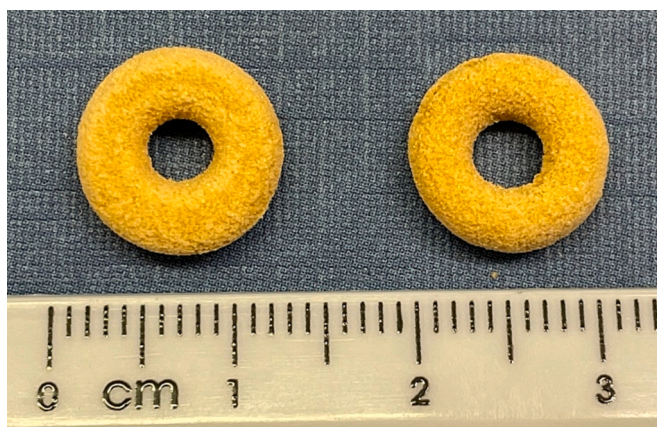

Fig. 5. Image of two torus printlets SLS90 (left) and SLS130 (right), printed at different laser speeds (90 mm/s and 130 mm/s).

Table 5
Physical properties of the SLS torus printlets.

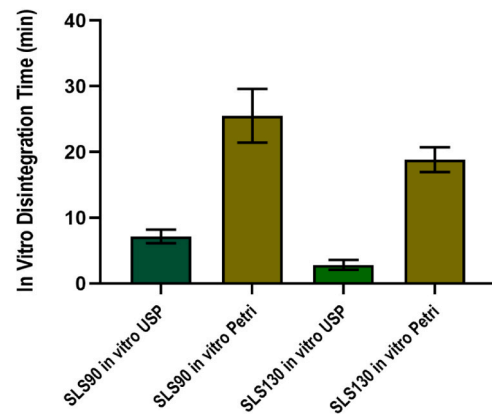| Formulation	Weight ± SD (mg) ($n = 12$)	Outer diameter ± SD (mm) ($n = 4$)	Height ± SD (mm) ($n = 4$)
SLS90	167.4 ± 0.01	11.06 ± 0.23	4.14 ± 0.22
SLS130	115.7 ± 0.00	10.98 ± 0.51	3.71 ± 0.32

Fig. 6. In vitro disintegration times obtained with the two different experimental setups (USP apparatus and petri dishes) ($n = 3$). Error bars represent standard deviation.

provides valuable information about the disintegration time and location of the formulation within the gastrointestinal tract [19]. The in vivo disintegration times were established by observing the loss of torus shape and the appearance of a dark trail on the MRI images (Figs. 7 and 8). The inclusion of 5% *w*/w MnCl$_2$ in the formulations facilitated the visualization of the printlets.

For the SLS90 formulation, the mean reported disintegration time was 17.3 ± 7.2 min, whereas for the SLS130 formulation it was 12.7 ± 6.8 min (Table 6). The obtained in vivo disintegration times align with the in vitro preliminary disintegration studies. As with the in vitro data, faster laser scanning speeds (130 mm/s) resulted in shorter disintegration times because of the porous structure obtained. On the other hand, slower laser scanning speeds (90 mm/s) led to a longer disintegration time due to the denser printlet structure obtained during printing. The supine position of the volunteers together with the sinking of the
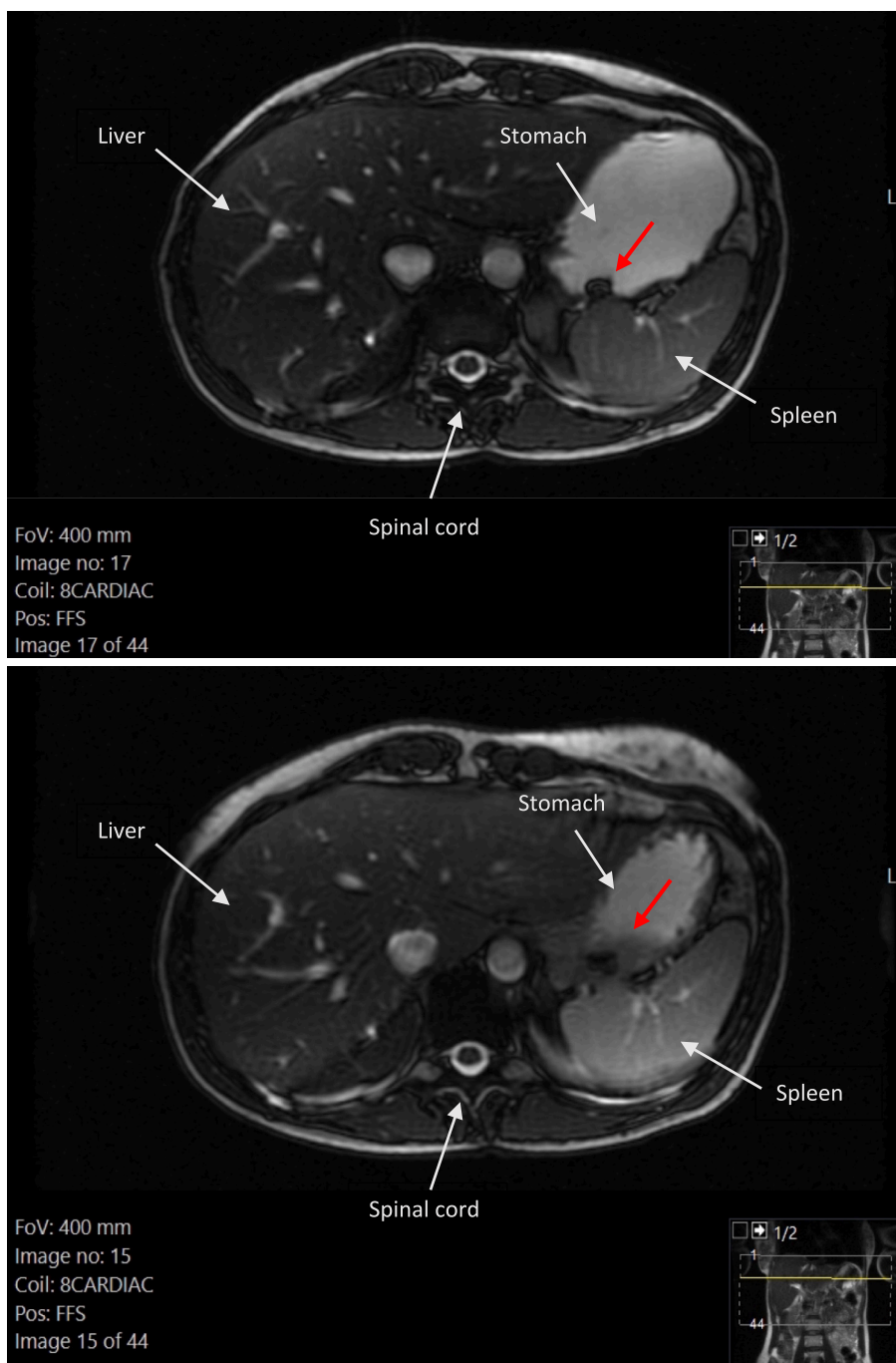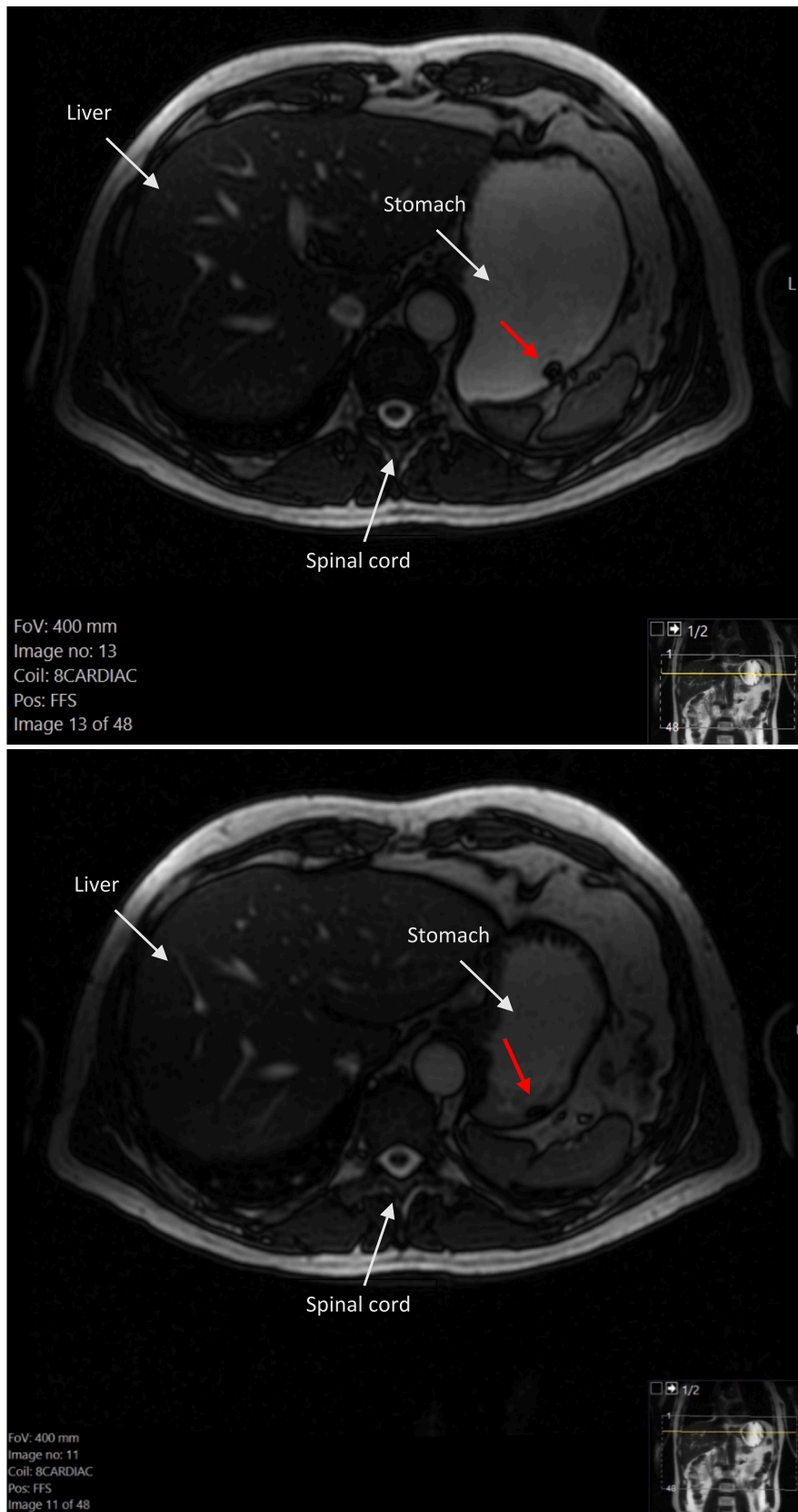
Fig. 7. Representative MRI images of the SLS90 formulation. The top image shows the formulation after ingestion where the torus shape of the printlet can be seen. At the bottom, image taken at the start of printlet disintegration (image taken 24 min after ingestion of the formulation). Red arrows indicate the printlet's location within the stomach. Additionally, a visible black trail resulting from the printlet disintegration is observed in the bottom image. (For interpretation of the references to colour in this figure legend, the reader is referred to the web version of this article.)

formulation in the stomach means that the printlet is closer to the pyloric region of the stomach. This may potentially facilitate an earlier emptying of the formulation through the pylorus. Moreover, the disintegration dynamics of the formulation could be also affected by sinking, as it may be exposed to gastric fluids and mechanical forces in the lower part of the stomach more quickly, leading to a faster disintegration compared to a formulation that remains buoyant in the upper part of the stomach. The implications of the supine position and sinking behaviour should be considered when assessing the performance of the formulation and interpreting results [38]. The fact that in two out of the six participants the results did not align with the expected disintegration times of

the formulations highlights the presence of physiological differences between volunteers. This serves as a reminder that various factors can influence in vivo disintegration times. Nonetheless, MRI has proven to be a valuable tool for studying the sensitivity of specific formulations to individual physiological factors.

Overall, this study successfully demonstrated the versatility of 3D printing in creating oral dosage forms with varying disintegration times. By using SLS 3D printing and adjusting laser scanning speeds, formulations with distinct disintegration rates were achieved. This finding was confirmed through both in vivo experiments and in vitro evaluations. Notably, the in vitro disintegration times obtained using the USP

Fig. 8. Representative MRI images of the SLS130 formulation. The top image shows the formulation after ingestion where the torus shape of the printlet can be visualised. At the bottom, image taken at the start of printlet disintegration (image taken 8 min after ingestion of the formulation). Red arrows indicate the printlet's location within the stomach. Additionally, a visible black trail resulting from the printlet disintegration is observed in the bottom image. (For interpretation of the references to colour in this figure legend, the reader is referred to the web version of this article.)

Table 6
In vivo disintegration times of torus formulations.

Volunteer	Disintegration time (min) SLS90	Disintegration time (min) SLS130
1	22.5	6.5
2	18	14
3	6.5	7
4	15	8
5	14.5	17.5
6	27.5	23.5
Mean ± SD	17.3 ± 7.2	12.7 ± 6.8

disintegration apparatus (7.2 ± 1.0 min for SLS90, and 2.8 ± 0.8 min for SLS130) did not align with the disintegration times observed in vivo (17.3 ± 7.2 min for SLS90, and 12.7 ± 6.8 min for SLS130). Conversely, disintegration studies conducted in petri dishes yielded disintegration times (25.5 ± 4.1 min for SLS90, and 18.8 ± 1.9 min for SLS130) more closely resembling those obtained in vivo.

While there are no previous in vivo disintegration studies using 3D printed dosage forms for comparison with the present study, data from in vivo disintegration studies with conventional tablets is available. In one study involving capsules and immediate-release tablets, the disintegration times were measured in vitro using a GastroDuo system, a biorelevant dissolution test device, based on drug concentrations in the outflow of the gastric cell [20]. The in vitro results were compared to data obtained from 14 volunteers using the salivary tracer technique. Both in vitro and in vivo methods determined the initial tablet or capsule disintegration time, defined by reaching a salivary drug concentration exceeding triple the limit of quantification. The study results revealed that the GastroDuo could detect certain differences between the tested immediate-release formulations. However, in comparison to in vivo data, there was greater in vitro variability for specific formulations. In another study, three distinct tablet formulations of paracetamol underwent in vitro and in vivo testing using MRI [18]. Whilst similarities were observed between the in vitro and in vivo behaviour, notable differences emerged, particularly in one formulation, a bilayer tablet. These differences can be explained by the forces of the in vivo conditions. In the in vitro setting, the bilayer tablet remained relatively intact. However, in vivo imaging revealed the disintegration of this layer, highlighting the impact of physiological conditions. In the case of a rapid release formulation, the tablet swelled to significantly bigger dimensions than its original size, both in vivo and in vitro. However, in the in vivo images, the tablet floated to the top of the stomach prior to disintegration.

These results suggest that not all in vivo scenarios were likely to occur under the controlled and standardised conditions of in vitro tests. It should be considered that some of these scenarios represented physiological extremes, which may only occur in certain patient populations or under specific conditions. Finally, the results presented in this study, along with insights from previous research, highlight the existing gap and the need for additional disintegration studies. Enhanced equipment should be developed to conduct in vitro disintegration and dissolution studies that more accurately replicate the diverse array of physiological conditions encountered by formulations in vivo. This is particularly crucial for 3D printed formulations, given their unique properties with distinctive disintegration and dissolution characteristics.

4. Conclusions

This is the first study to investigate the in vivo disintegration of 3D printed oral dosage forms in human volunteers. Following preliminary investigations, the optimal HPC grade and MRI contrast agent were selected to prepare further placebo printlets specifically intended for in vivo studies. Two SLS 3D printed formulations were administered to 6 human volunteers, and their in vivo disintegration times were assessed using MRI. The formulation printed using the lowest laser scanning speed (90 mm/s) exhibited an average in vivo disintegration time of 17.3 ± 7.2 min, whereas the formulation printed with the highest laser

scanning speed (130 mm/s) disintegrated in 12.7 ± 6.8 min. Disintegration times obtained in vitro using the petri dish-based setup (25.5 ± 4.1 min for SLS90, and 18.8 ± 1.9 min for SLS130) more closely resembled those obtained in vivo. However, the in vivo disintegration times were not directly correlated with those obtained through in vitro assessments using the USP apparatus and the petri dish-based setup, highlighting the need for the development of better in vitro disintegration tests to assess behaviour of 3D printed formulations. Overall, this study demonstrates the capability of SLS 3D printing technology to produce formulations with diverse in vivo disintegration times, and the utility of MRI in assessing these disintegration profiles.

CRediT authorship contribution statement

Iria Seoane-Viaño: Writing – review & editing, Writing – original draft, Visualization, Validation, Methodology, Investigation, Formal analysis, Data curation, Conceptualization. **Tania Pérez-Ramos:** Writing – review & editing, Visualization, Validation, Software, Project administration, Methodology, Investigation, Data curation, Conceptualization. **Jiaqi Liu:** Writing – original draft, Visualization, Validation, Methodology, Investigation, Formal analysis, Data curation. **Patricija Januskaite:** Writing – review & editing, Visualization, Validation, Methodology, Investigation, Formal analysis, Data curation. **Elena Guerra-Baamonde:** Visualization, Validation, Software, Methodology, Investigation, Data curation. **Jorge González-Ramírez:** Validation, Supervision, Software, Resources, Project administration. **Manuel Vázquez-Caruncho:** Validation, Supervision, Software, Resources, Project administration. **Abdul W. Basit:** Writing – review & editing, Validation, Supervision, Resources, Project administration, Funding acquisition, Formal analysis, Data curation, Conceptualization. **Alvaro Goyanes:** Writing – review & editing, Validation, Supervision, Resources, Project administration, Funding acquisition, Formal analysis, Data curation, Conceptualization.

Declaration of Competing Interest

The authors declare the following financial interests/personal relationships which may be considered as potential competing interests. Alvaro Goyanes reports a relationship with FabRx that includes equity or stocks. Abdul Basit reports a relationship with FabRx that includes equity or stocks.

Data availability

Data will be made available on request.

Appendix A. Supplementary data

Supplementary data to this article can be found online at https://doi.org/10.1016/j.jconrel.2023.11.022.

References

[1] I. Seoane-Viaño, et al., Translating 3D printed pharmaceuticals: from hype to real-world clinical applications, Adv. Drug Deliv. Rev. 174 (2021) 553–575.
[2] G. Chen, et al., Pharmaceutical applications of 3D printing, Addit. Manuf. 34 (2020), 101209.
[3] I. Seoane-Viaño, et al., To infinity and beyond: strategies for fabricating medicines in outer space, Int. J. Pharmaceut.: X 4 (2022), 100121.
[4] M. Cui, et al., Opportunities and challenges of three-dimensional printing technology in pharmaceutical formulation development, Acta Pharm. Sin. B 11 (8) (2021) 2488–2504.

[5] S.J. Trenfield, et al., Prediction of solid-state form of SLS 3D printed medicines using NIR and Raman spectroscopy, Pharmaceutics 14 (3) (2022).

[6] Y.A. Gueche, et al., Selective laser sintering (SLS), a new chapter in the production of solid Oral forms (SOFs) by 3D printing, Pharmaceutics 13 (8) (2021).

[7] K. Englezos, et al., 3D printing for personalised medicines: implications for policy and practice, Int. J. Pharm. 635 (2023), 122785.

[8] A. Awad, et al., Advances in powder bed fusion 3D printing in drug delivery and healthcare, Adv. Drug Deliv. Rev. 174 (2021) 406–424.

[9] E. Tikhomirov, et al., Selective laser sintering additive manufacturing of dosage forms: effect of powder formulation and process parameters on the physical properties of printed tablets, Int. J. Pharm. 635 (2023), 122780.

[10] F. Fina, et al., Fabricating 3D printed orally disintegrating printlets using selective laser sintering, Int. J. Pharm. 541 (1–2) (2018) 101–107.

[11] R. Thakkar, et al., Impact of laser speed and drug particle size on selective laser sintering 3D printing of amorphous solid dispersions, Pharmaceutics 13 (8) (2021).

[12] N. Allahham, et al., Selective laser sintering 3D printing of orally disintegrating Printlets containing ondansetron, Pharmaceutics 12 (2) (2020).

[13] T. Evgenii, et al., Impact of polymer chemistry on critical quality attributes of selective laser sintering 3D printed solid oral dosage forms, Int. J. Pharm. X 6 (2023), 100203.

[14] G.V. Salmoria, et al., The effects of laser energy density and particle size in the selective laser sintering of polycaprolactone/progesterone specimens: morphology and drug release, Int. J. Adv. Manuf. Technol. 66 (5) (2013) 1113–1118.

[15] D. Markl, J.A. Zeitler, A review of disintegration mechanisms and measurement techniques, Pharm. Res. 34 (5) (2017) 890–917.

[16] J. Al-Gousous, P. Langguth, Oral solid dosage form disintegration testing - the forgotten test, J. Pharm. Sci. 104 (9) (2015) 2664–2675.

[17] G. Abdelbary, et al., Determination of the in vitro disintegration profile of rapidly disintegrating tablets and correlation with oral disintegration, Int. J. Pharm. 292 (1–2) (2005) 29–41.

[18] L. Curley, et al., Magnetic resonance imaging to visualize disintegration of Oral formulations, J. Pharm. Sci. 106 (3) (2017) 745–750.

[19] M. Sager, et al., Combined application of MRI and the salivary tracer technique to determine the in vivo disintegration time of immediate release formulation administered to healthy, fasted subjects, Mol. Pharm. 16 (4) (2019) 1782–1786.

[20] M. Sager, et al., Comparison of in vitro and in vivo results using the GastroDuo and the salivary tracer technique: immediate release dosage forms under fasting conditions, Pharmaceutics 11 (12) (2019).

[21] A. Rump, et al., In vivo evaluation of a gastro-resistant HPMC-based "next generation enteric" capsule, Pharmaceutics 14 (10) (2022).

[22] S. Sulaiman, et al., Application of in vivo MRI imaging to track a coated capsule and its disintegration in the gastrointestinal tract in human volunteers, Pharmaceutics 14 (2) (2022).

[23] N. Gómez-Lado, et al., Gastrointestinal tracking and gastric emptying of coated capsules in rats with or without sedation using CT imaging, Pharmaceutics 12 (1) (2020).

[24] D. Bertoli, et al., Quantification of gastric emptying with magnetic resonance imaging in healthy volunteers: a systematic review, Neurogastroenterol. Motil. 34 (12) (2022), e14371.

[25] D.M. Mudie, et al., Quantification of gastrointestinal liquid volumes and distribution following a 240 mL dose of water in the fasted state, Mol. Pharm. 11 (9) (2014) 3039–3047.

[26] M. Grimm, et al., Comparing the gastric emptying of 240 mL and 20 mL water by MRI and caffeine salivary tracer technique, Eur. J. Pharm. Biopharm. 184 (2023) 150–158.

[27] M. Sager, et al., In vivo characterization of enTRinsicTM drug delivery technology capsule after intake in fed state: a cross-validation approach using salivary tracer technique in comparison to MRI, J. Control. Release 313 (2019) 24–32.

[28] A. Goyanes, et al., Patient acceptability of 3D printed medicines, Int. J. Pharm. 530 (1) (2017) 71–78.

[29] H. Sunada, Y. Bi, Preparation, evaluation and optimization of rapidly disintegrating tablets, Powder Technol. 122 (2) (2002) 188–198.

[30] A. Awad, et al., 3D printed tablets (Printlets) with braille and moon patterns for visually impaired patients, Pharmaceutics 12 (2) (2020).

[31] Y. Zhang, et al., Investigating the use of magnetic nanoparticles as alternative sintering agents in selective laser sintering (SLS) 3D printing of Oral tablets, ACS Biomater. Sci. Eng. 9 (6) (2023) 2924–2936.

[32] H. Barthel, L. Rösch, J. Weis, Fumed Silica - Production, Properties, and Applications, in Organosilicon Chemistry II, 1995, pp. 761–778.

[33] W. Weitschies, C.G. Wilson, In vivo imaging of drug delivery systems in the gastrointestinal tract, Int. J. Pharm. 417 (1–2) (2011) 216–226.

[34] F. Fina, et al., Selective laser sintering (SLS) 3D printing of medicines, Int. J. Pharm. 529 (1) (2017) 285–293.

[35] C. Luebbert, E. Stoyanov, G. Sadowski, Phase behavior of ASDs based on hydroxypropyl cellulose, Int. J. Pharm. X 3 (2021), 100070.

[36] M. Schmid, A. Amado, K. Wegener, Polymer powders for selective laser sintering (SLS), AIP Conf. Proc. 1664 (1) (2015), 160009.

[37] USP 43-NF 38; 701 Disintegration General Chapter. The United States Pharmacopeial Convention: Rockville, ML, USA, 2020.

[38] M. Grimm, et al., Characterization of the gastrointestinal transit and disintegration behavior of floating and sinking acid-resistant capsules using a novel MRI labeling technique, Eur. J. Pharm. Sci. 129 (2019) 163–172.